Results in Physics 8 (2018) 146–152

Contents lists available at ScienceDirect

Results in Physics

journal homepage: www.journals.elsevier.com/results-in-physics

Investigation on AlP as the heterogeneous nucleus of Mg_2Si in Al–Mg_2Si alloys by experimental observation and first-principles calculation

Jiayue Sun [a], Chong Li [a,*], Xiangfa Liu [b], Liming Yu [a], Huijun Li [a], Yongchang Liu [a,*]

[a] State Key Lab of Hydraulic Engineering Simulation and Safety, School of Materials Science and Engineering, Tianjin University, Tianjin 300350, China
[b] Key Laboratory of Liquid-Solid Structural Evolution and Processing of Materials, Ministry of Education, Shandong University, Jinan 250061, China

ARTICLE INFO

Article history:
Received 27 September 2017
Received in revised form 20 November 2017
Accepted 20 November 2017
Available online 26 November 2017

Keywords:
AlP
Al–Mg_2Si alloys
First-principles calculation
Heterogeneous nucleus

ABSTRACT

The microstructural evolution of primary Mg_2Si in Al–20%Mg_2Si with Al–3%P master alloy was observed by scanning electron microscope. And the interfacial properties of AlP/Mg_2Si interface were investigated using first-principles calculations. The calculation results show that AlP(1 0 0)/Mg_2Si(2 1 1) and AlP(3 3 1)/Mg_2Si(1 1 0) interfaces can form steadily. P-terminated AlP(1 0 0)/Mg_2Si(2 1 1) interface with the largest work of adhesion (4.13 J/m^2) is theoretically the most stable. The interfacial electronic structure reveals that there are covalent Si–Al, Si–P and Mg–P bonds existing between AlP and Mg_2Si slabs. Due to the AlP particles as effective heterogeneous nucleus of Mg_2Si, primary Mg_2Si particles change from dendrite to octahedron/truncated octahedron, and their sizes decrease to ~20 μm.

Introduction

Magnesium silicide, Mg_2Si, is a hard intermetallic compound with high melting point (1085 °C). It exhibits low density (1.99 × 10^3 kgm^{-3}), low thermal expansion coefficient (7.5 × 10^{-6} K^{-1}), high hardness (4.5 × 10^9 Nm^{-2}) and reasonably high elastic modulus (120 GP) [1,2]. As particle-reinforced structural materials, Al–Mg_2Si alloys have been widely used in many fields with their excellent properties [3]. In as-cast hypereutectic Al–Mg_2Si alloys, primary Mg_2Si shows enormous dendrite (irregular shape) or fine polyhedron (perfect/imperfect octahedron and hopper).

The mechanical properties of Al–Mg_2Si alloys are dependent upon the morphology, size and distribution of Mg_2Si phase. Addition of refiners or modifiers is an effective method and has been adopted to control primary Mg_2Si particles with desirable shapes and sizes, such as P, Sr, Sb, Na, Li [4–14]. In the previous paper, it was found that AlP particles could act as the nuclei of primary Mg_2Si [12]. Coarse Mg_2Si dendrites evolve into numerous fine octahedron or truncated octahedron particles by increase of the Mg_2Si crystal nuclei, resulting in the increase of tensile strength of Al–Mg_2Si alloys [3,12]. The effectiveness of AlP as the heterogeneous nucleus of Mg_2Si has also been studied by mismatch theory [12]. However, mismatch theory is limited on analyzing the effectiveness of heterogeneous nucleation but can not study the nucleation interfacial properties directly [15,16].

In recent years, first-principles method based on density functional theory (DFT) has been widely utilized to study the nucleation and interface [17–19], including the interface atomic arrangement rule and bonding condition, interfacial adhesion work and interfacial energy during the nucleation process. S. Liu et al. [20] calculated the interface properties of $Fe_3Cr_4C_3$ (0 0 0 1)/TiC (1 1 1) interface by first-principles method, and revealed that TiC in Fe–Cr–C–Ti alloy was the heterogeneous nucleus of primary M_7C_3. First-principles calculations were also employed to research the Mg/Al_2MgC_2 heterogeneous nucleation interfaces by H. L Wang et al. [21]. The interfacial structure and electronic properties were studied, and the results suggested that Al_2MgC_2 could be the potent crystal nucleus of α-Mg grains in the solidification of carbon-inoculated Mg–Al alloy. Y.F. Han [22] calculated the atomic structure, adhesion, and interfacial energy of Al/TiB_2 interfaces, and analyzed the mechanism of TiB_2 as the heterogeneous nuclei of the α-Al phase in Al alloys by first-principles.

In this work, the morphological evolution of primary Mg_2Si in Al–20%Mg_2Si alloy with the addition of Al–3%P master alloy was observed by experimental method. Moreover, the electronic structure and adhesion work of AlP/Mg_2Si interfaces (with small lattice disregistry) were calculated using the first-principles method and stacking sequence of Mg, Si atoms on AlP substrate was discussed, which can provide theoretical basis for AlP as the heterogeneous nucleus of Mg_2Si from the energetic theory.

* Corresponding authors.
E-mail addresses: lichongme@tju.edu.cn (C. Li), licmtju@163.com (Y. Liu).

https://doi.org/10.1016/j.rinp.2017.11.025
2211-3797/

Experimental procedures and theoretical calculation

Experimental procedures

The Al–20%Mg_2Si alloy used in this study was prepared by casting. Commercial pure Al (99.7%, wt.% in this work), commercial pure crystalline Si (99.9%) and commercial pure Mg (99.8%) were used as raw materials to prepare this experimental alloy in a 25 kW medium frequency induction furnace. The Al–20%Mg_2Si alloy was remelted at 800 °C and held at this temperature for 30 min in a 5 kW electric resistant-heating furnace, and then the melt was poured into a cast iron mold to produce ingots. In order to investigate the influence of phosphorus on Mg_2Si phases, a part of Al–20%Mg_2Si alloy was treated with addition of 3% Al–3%P master alloy at 800 °C and held for 30 min, and then was poured into a cast iron mold to obtain ingots.

All metallographic specimens were cut at the same position of the tabulate samples and then mechanically polished using standard processes. A NaOH water solution (15%) was used as etchant to extract primary Mg_2Si phase from Al–20%Mg_2Si alloy for direct observation of its morphologies. Scanning electron microscope (SEM) (Hitachi Model No. S4800) was carried out to investigate the microstructure characteristics of the specimens.

Computational details

Calculations in this work were performed using the projector augmented wave (PAW) formalism of density functional theory (DFT) [23], as implemented in Vienna ab initio Simulation Package (VASP) [24]. Generalized gradient approximation (GGA) in the form of PW91 was used for the exchange-correlation functional [25]. The tetrahedron method with Blöchl corrections was adopted, and the width of smearing was chosen as 0.1 eV. A plane-wave basis with an energy cutoff of 400 eV was adopted for all the calculations.

AlP and Mg_2Si crystals belong to face-centered cubic structure, and their space groups are F-43m and Fm3m, respectively. According to the lattice disregistry theory [12,26], possible coherent interfaces between AlP and Mg_2Si $((3\,3\,1)_{AlP}/(1\,1\,0)_{Mg_2Si}$, $(1\,0\,0)_{AlP}/(2\,1\,1)_{Mg_2Si})$ can be obtained, and the values of disregistry are 1.10% and 3.87%, respectively. It indicates that AlP can potentially act as heterogeneous nuclei for Mg_2Si phase in these orientation relationships. Therefore, the interface orientation relationships mentioned above were adopted for theoretical study. To ensure the slabs in the interface structures thick enough to show bulk-like characteristics, the convergence tests were conducted on the AlP(3 3 1), AlP(1 0 0), Mg_2Si(1 1 0) and Mg_2Si(2 1 1). It was found that surface energies and interlayer relaxations had good convergence when the slabs thicknesses of AlP(3 3 1), AlP(1 0 0), Mg_2Si (1 1 0) and Mg_2Si(2 1 1) were larger than 11, 5, 5 and 5, respectively. The Brillouin zone was sampled using Monkhorst–Pack scheme [27] with $9 \times 9 \times 1$ k-point grid for the structural relaxation of AlP/Mg_2Si interfaces, and $11 \times 11 \times 1$ for static calculations and electronic structure calculations of all the systems. A vacuum layer (10 Å) was placed on the top of Mg_2Si slabs to separate the free surfaces of Mg_2Si and AlP slabs with an in-plane periodicity to prevent other atomic interaction among the layers.

In order to obtain the stacking sequence of Mg and Si atoms on the AlP surfaces during the formation of the interfaces, adsorption model was adopted. The adsorbed layers were formed by crystallization phase atoms. A $7 \times 7 \times 1$ k-point mesh was used for the calculation of adsorption energy. In the vertical direction, a vacuum layer of about 10 Å in thickness was introduced for all the surfaces.

The geometry optimization was not finished until the Hellmann-Feynman forces less than 0.01 eV/Å for all models. VESTA was used for structure and electronic visualization and analysis [28].

Results and discussion

Effect of Al–3%P master alloy on the microstructure of Al–20%Mg_2Si alloy

The microstructure of as-cast Al–20%Mg_2Si alloy is presented in Fig. 1. From Fig. 1a, it can be seen that the primary Mg_2Si shows different coarse irregular shapes (two-dimensional observation). The three-dimensional morphologies of the extracted primary Mg_2Si are shown in Fig. 1b–d. These Mg_2Si dendrites exhibit a variety of interesting shapes with inconspicuous crystallographic features of surfaces.

After addition of 3% Al–3%P master alloy in Al–20%Mg_2Si alloy, morphology and size of primary Mg_2Si are obviously changed (Fig. 2a and b). All coarse dendritic Mg_2Si particles disappear and evolve into octahedron (Fig. 2c) and truncated octahedron (Fig. 2d), and their size decreases to ~20 μm. The AlP compound existing in Al–3%P master alloy can act as effective heterogeneous nucleus of Mg_2Si. The rising of nuclei evidently results in an increase in Mg_2Si particles, which leads the growth rate of preferential growth ⟨1 0 0⟩ directions to decelerate [12]. As a result, the enormous dendrite can not be formed along the preferential growth directions, and Mg_2Si grows in the manner of octahedron and truncated octahedron.

Interfaces of AlP/Mg_2Si

In order to confirm the effectiveness of AlP as the heterogeneous nucleus of Mg_2Si, interfacial adhesion work and electronic structures of AlP/Mg_2Si nucleation interfaces were researched by first-principles calculation. According to the terminated types of atoms, AlP(1 0 0) surface can be divided into Al-terminated and P-terminated surfaces. Therefore, three interface models between AlP and Mg_2Si slabs were built according to the results of convergence tests to identify the favorable structure (shown in Fig. 3). All atomic coordinates were allowed for full relaxation. The work of adhesion (W_{ad}) is considered as an important interfacial property to investigate the interface interiors. The value of W_{ad} can evaluate the stability of the interface, and it is defined as the reversible work for separating an interface into two free surfaces, neglecting plastic and diffuse degrees of freedom. The larger the W_{ad} is, the stronger the interface interaction is. The work of adhesion of AlP/Mg_2Si interfaces can be given by [29]:

$$W_{ad} = \left(E^{tot}_{AlP} + E^{tot}_{Mg_2Si} - E^{tot}_{AlP/Mg_2Si}\right)/A \quad (1)$$

where E^{tot}_{AlP}, $E^{tot}_{Mg_2Si}$, and E^{tot}_{AlP/Mg_2Si} are the total energy of the relaxed AlP slabs, Mg_2Si slabs and AlP/Mg_2Si interface system, respectively. A represents the area of interface system.

The values of optimal W_{ad} for different interface geometries are listed in Table 1. From Table 1, it can be obtained that all the values of W_{ad} are positive, indicating that the three AlP/Mg_2Si interfaces all can form steadily. The value of W_{ad} of AlP/Mg_2Si interface exhibits the following sequence: P-terminated AlP(1 0 0)/Mg_2Si(2 1 1) interface (4.13 J/m^2) > Al-terminated AlP(1 0 0)/Mg_2Si(2 1 1) interface (2.73 J/m^2) > AlP(3 3 1)/Mg_2Si(1 1 0) (1.03 J/m^2). The value of W_{ad} of AlP(1 0 0)/Mg_2Si(2 1 1) is higher than that of AlP(3 3 1)/Mg_2Si(1 1 0), namely, AlP(1 0 0)/Mg_2Si(2 1 1) is more stable than AlP(3 3 1)/Mg_2Si(1 1 0). For the AlP(1 0 0), the adhesion work W_{ad} of P-terminated interface is larger than that of Al-terminated one, suggesting that the binding strength of P-terminated interface is stronger than that of the latter. Meanwhile, the interfacial separation of three interfaces before and after structural relaxation is

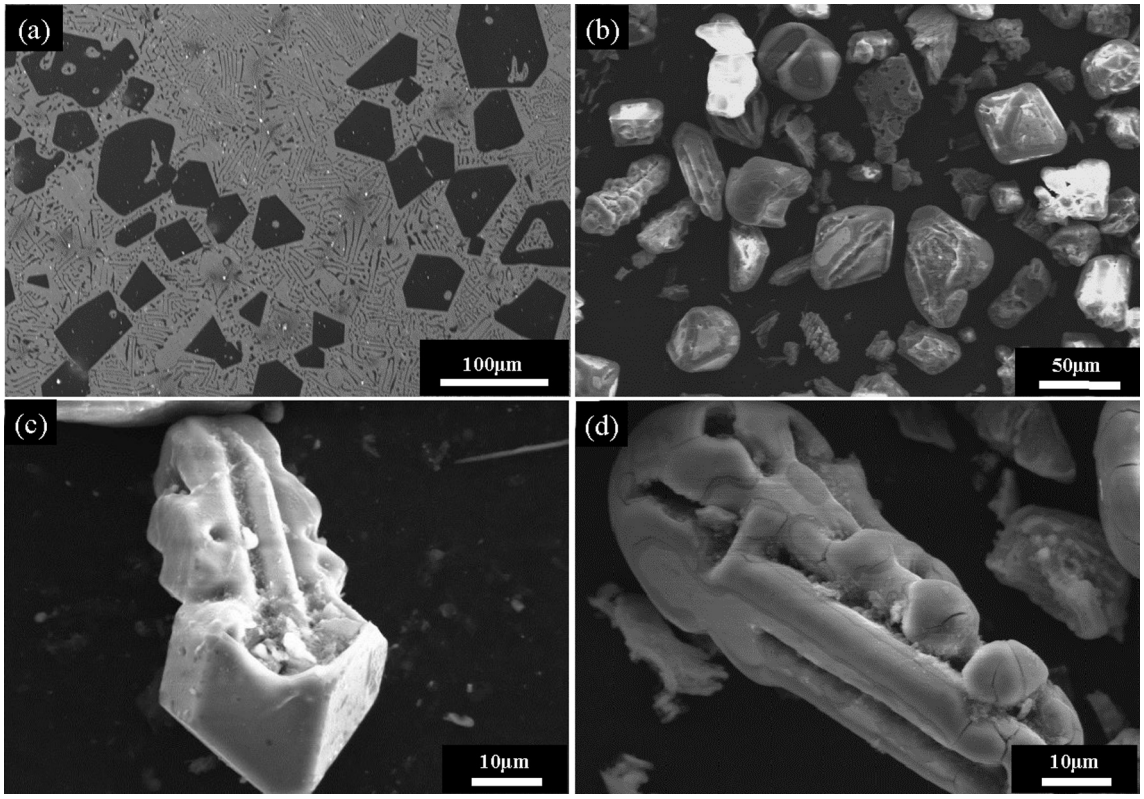

Fig. 1. Microstructures of as-cast Al–20%Mg_2Si alloy: (a) two-dimensional morphologies; (b–d) three-dimensional morphologies.

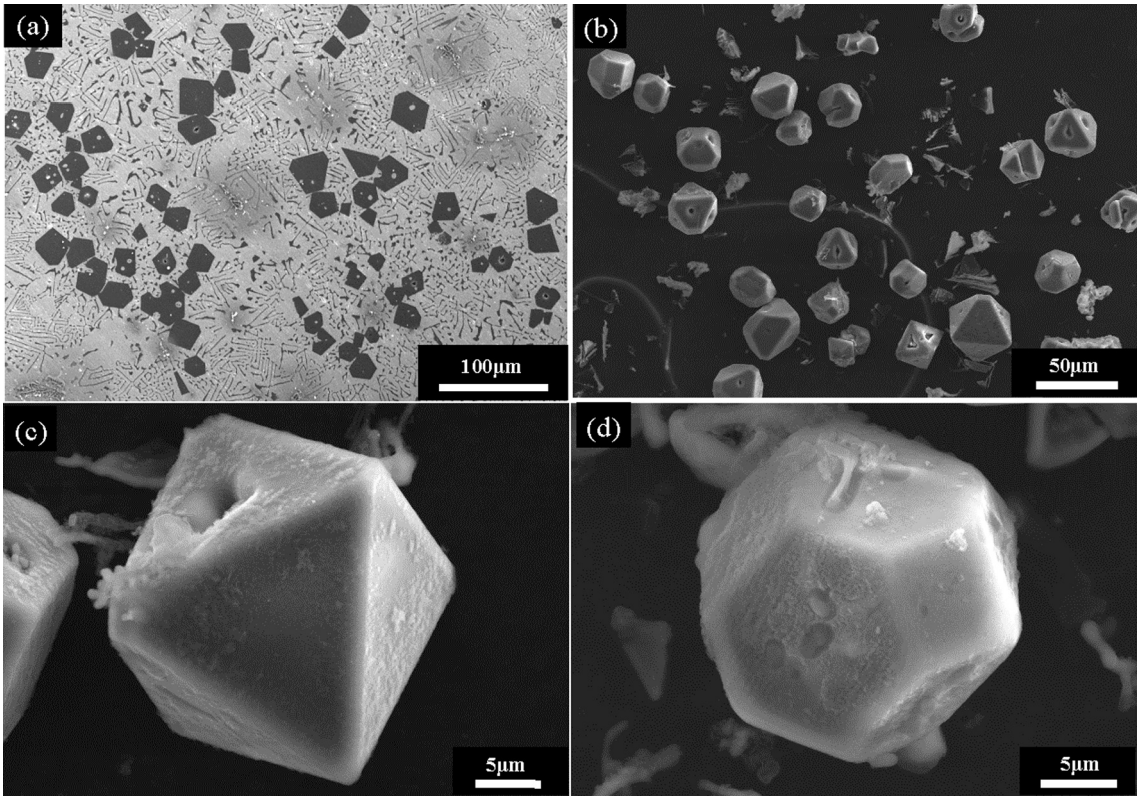

Fig. 2. Microstructures of Al–20%Mg_2Si alloy with addition of 3%Al–3%P master alloy: (a) two-dimensional morphologies; (b–d) three-dimensional morphologies.

also listed in Table 1. The d_0 and d_1 are the interfacial distances before and after the relaxation, respectively. It can be seen that the interfacial distances of three interfaces before relaxation are equivalent (2.50 Å). After structural relaxation, the interfacial distances of the three interfaces all decrease. In addition, the interfacial distance of interface (c) is the smallest (0.78 Å) among the

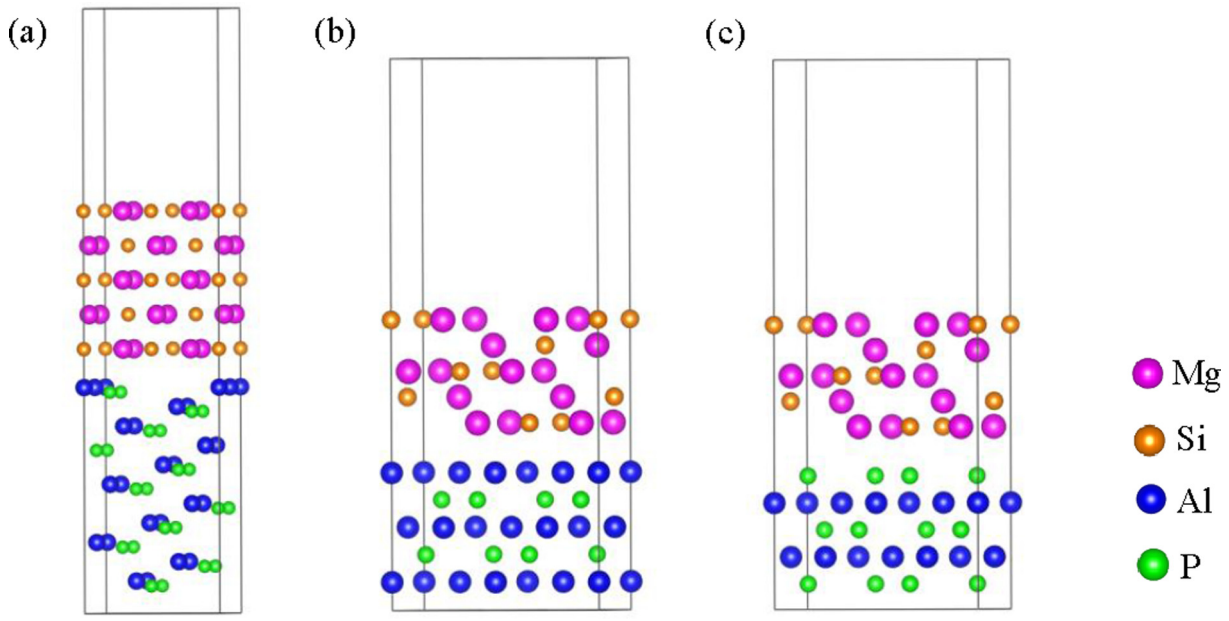

Fig. 3. Three models of AlP/Mg_2Si interfaces: (a) AlP(3 3 1)/Mg_2Si(1 1 0); (b) Al-terminated AlP(1 0 0)/Mg_2Si(2 1 1); (c) P-terminated AlP(1 0 0)/Mg_2Si(2 1 1).

Table 1
The work of adhesion (W_{ad}) and interfacial distance before (d_0) and after (d_1) relaxation for different interfaces.

Interface	d_0 (Å)	d_1 (Å)	W_{ad} (J/m^2)
AlP(3 3 1)/Mg_2Si(1 1 0)	2.50	1.71	1.03
Al-terminated AlP(1 0 0)/Mg_2Si(2 1 1)	2.50	1.10	2.73
P-terminated AlP(1 0 0)/Mg_2Si(2 1 1)	2.50	0.78	4.13

three kinds of interfaces, indicating that P-terminated AlP(1 0 0) surface is more reactive and ready to form bonds. The reason may be that Mg and Si atoms in Mg_2Si tend to have strong interaction with P atoms in AlP(1 0 0) slabs, and the orientation relationships lead to a large W_{ad}. Thus, the P-terminated AlP(1 0 0)/Mg_2Si (2 1 1) interface is considered to be the most favorable structure in the three interface models in the view of work of adhesion.

In order to further ascertain the interfacial binding, the electronic structures of the three AlP/Mg_2Si interfaces were also explored, which can be discussed by charge density difference and partial density of states (PDOS). The charge density difference can be calculated by the following formula:

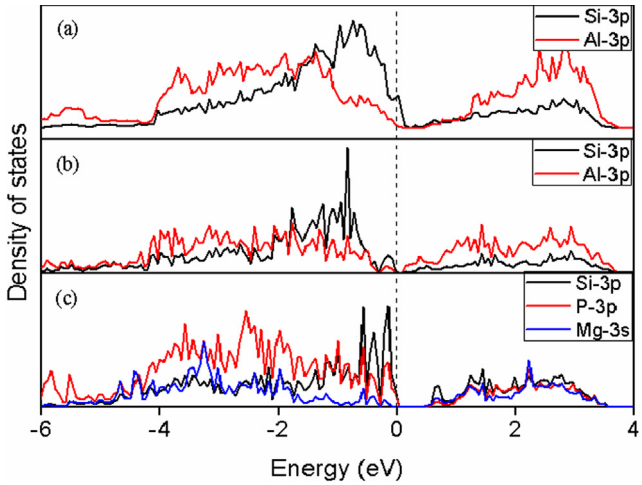

Fig. 5. The partial density of states (PDOS) of the atoms (marked by arrows in Fig. 4) at the interface: (a) AlP(3 3 1)/Mg_2Si(1 1 0); (b) Al-terminated AlP(1 0 0)/Mg_2Si(2 1 1); (c) P-terminated AlP(1 0 0)/Mg_2Si(2 1 1). The PDOS of Al 3p and Mg 3 s are enhanced by 3 times to show clearly. Dotted line represents Fermi energy level.

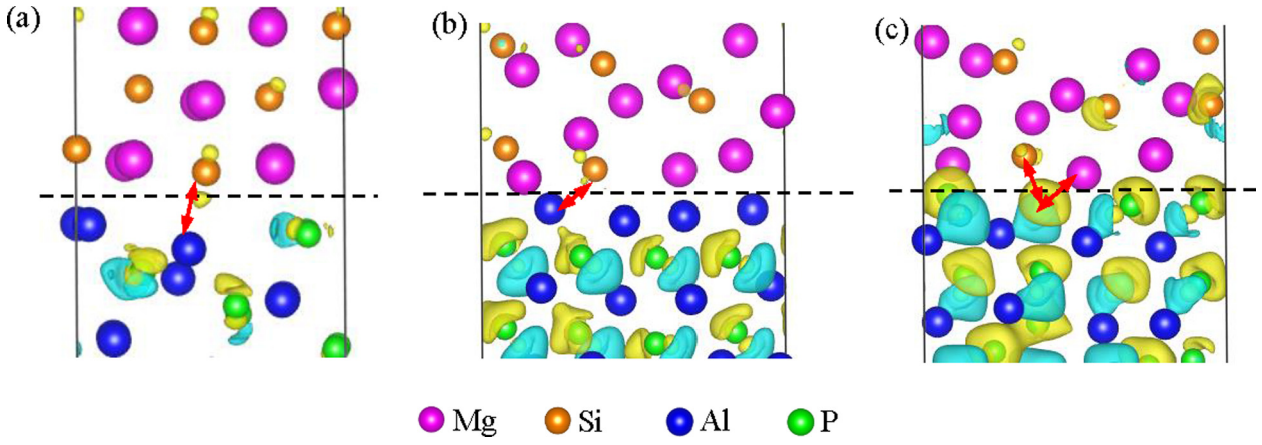

Fig. 4. Charge density difference map of AlP/Mg_2Si interfaces: (a) AlP(3 3 1)/Mg_2Si(1 1 0); (b) Al-terminated AlP(1 0 0)/Mg_2Si(2 1 1); (c) P-terminated AlP(1 0 0)/Mg_2Si(2 1 1). The isosurface value is 0.05 e/Å^3. Yellow and blue represent the enrichment and loss of electrons, respectively. Dotted line indicates the interface position. (For interpretation of the references to colour in this figure legend, the reader is referred to the web version of this article.)

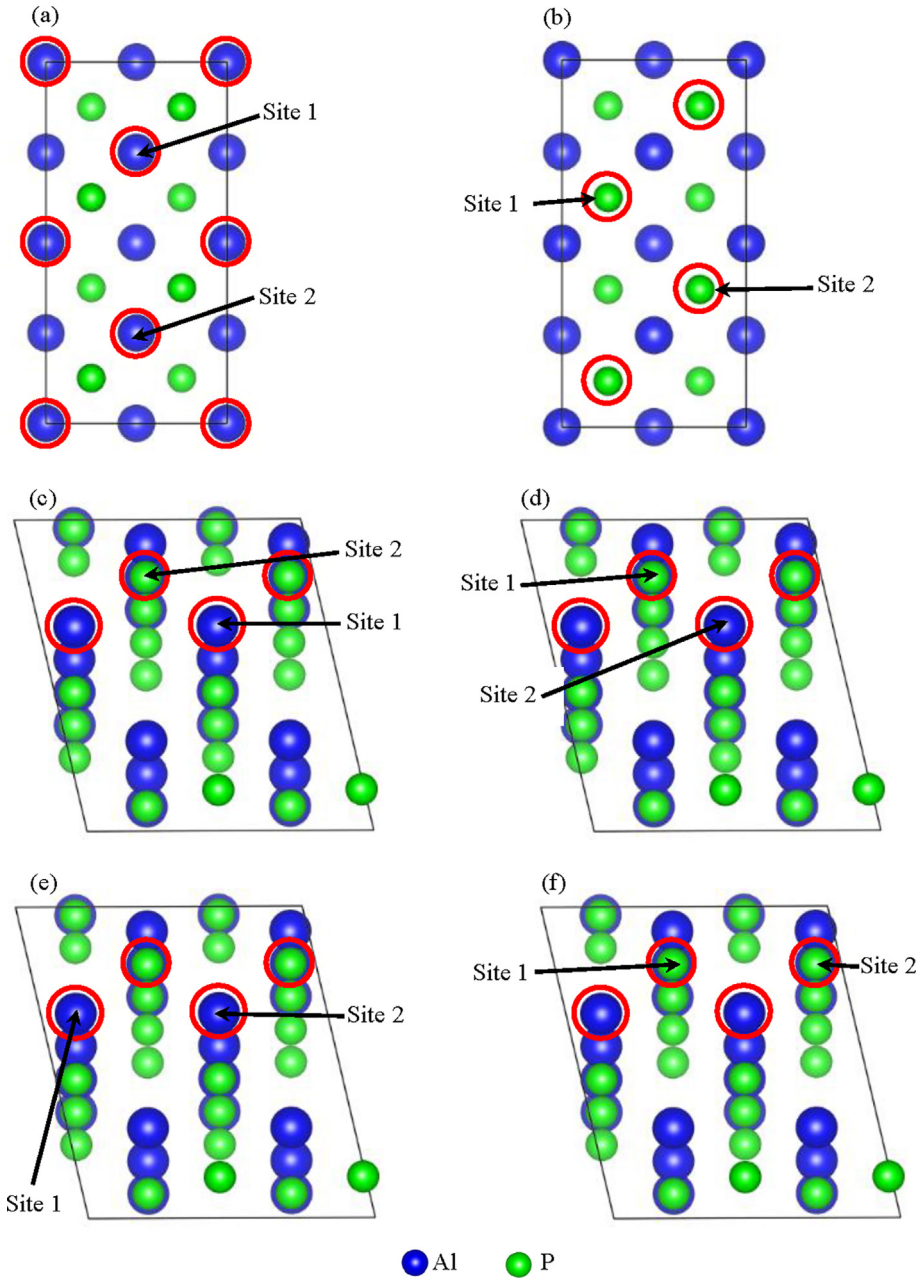

Fig. 6. Top view of adsorption sites: (a) Al-terminated AlP(1 0 0); (b) P-terminated AlP(1 0 0); (c–f) AlP(3 3 1). Mg, Si atoms are on top-site of Al or P, and site 1 stands for Mg atom, site 2 stands for Si atom. Atoms in red circles are at the first atomic layer. (For interpretation of the references to colour in this figure legend, the reader is referred to the web version of this article.)

Table 2
Data of adsorption energy (E_{ads}) of different adsorption models.

Surface	Adsorption site	E_{ads} (eV)
AlP(1 0 0)	(a) Al-terminated: Mg, Si on top of Al	5.20
	(b) P-terminated: Mg, Si on top of P	6.98
AlP(3 3 1)	(c) Mg on top of Al, Si on top of P	4.60
	(d) Mg on top of P, Si on top of Al	4.67
	(e) Mg, Si on top of Al	5.14
	(f) Mg, Si on top of P	3.78

$$\Delta\rho = \rho_{total} - \rho_{AlP} - \rho_{Mg_2Si} \quad (2)$$

where ρ_{total} is the total charge density of AlP/Mg_2Si interface, ρ_{AlP} and ρ_{Mg_2Si} represent the charge density of isolated AlP slabs and Mg_2Si slabs, respectively.

After relaxation, the charge density difference of AlP/Mg_2Si interfaces is shown in Fig. 4. It can be seen that chemical bonds are formed between interfacial atoms of Mg_2Si and AlP sides, while the strength of bonding is different. For AlP(3 3 1)/Mg_2Si(1 1 0), a small charge accumulation region exists between interfacial Si atoms of Mg_2Si side and Al atoms of AlP side (Fig. 4a), indicating that only a relatively weak chemical bond is formed at the interface. Also for Al-terminated AlP(1 0 0)/Mg_2Si(2 1 1) interface, there is the similar situation (Fig. 4b). In Fig. 4c, the bonding strength of P-terminated AlP(1 0 0)/Mg_2Si(2 1 1) interface is obviously stronger than that of the other two. Moreover, chemical bonds with considerable strength are formed among the interfacial Mg, Si atoms of Mg_2Si side and P atoms of AlP side.

The partial density of states (PDOS) was adopted in this work to give further insight into the details of the interaction between the AlP slabs and Mg_2Si slabs. Fig. 5 shows PDOS of the atoms (marked

by arrows in Fig. 4) at the interface. Peaks of Si-3p and Al-3p orbits (Fig. 5a and b) are superposed near the Fermi energy, illustrating that Si-Al covalent bonds are formed in the two interfaces. The PDOS analysis of P-terminated AlP(1 0 0)/Mg_2Si(2 1 1) interface is shown in Fig. 5c. It can be seen that the covalent bonds with great strength exist in interfacial atoms due to the electron orbital hybridization in valence band between the 3p states of Si and P, as well as 3s states of Mg atom and P-3p states. This is in good agreement with the charge density difference analysis.

Stacking sequence of Mg, Si atoms on AlP

Based on the results calculated above, adsorption model was put forward to simulate the stacking sequence of Mg, Si atoms on AlP interfaces. In this particular study, Mg and Si atoms on the AlP substrate were regarded as an adsorbed layer. For simplicity, only one Mg atom and one Si atom were used for all the models in this part, and Mg and Si atoms were on top-site of Al or P atoms (shown in Fig. 6). The adsorption energy of Mg, Si atoms is defined as follows:

$$E_{ads} = E_{AlP} + E_{atoms} - E_{AlP/atoms} \quad (3)$$

where E_{AlP} and $E_{AlP/atoms}$ represent the energy of clean AlP slabs and the slabs with adsorbed Mg and Si atoms, respectively. E_{atoms} is the energy of Mg and Si atoms. It can be inferred that the adsorption model is stable when E_{ads} is positive. And the more positive value of E_{ads} indicates the stronger interaction between the Mg, Si atoms and AlP substrate surface.

The calculated results of adsorption energy for the six adsorption models (shown in Fig. 6) are given in Table 2. The E_{ads} of Mg, Si atoms and AlP surfaces are all positive, and it is inferred that the adsorption between Mg, Si atoms and AlP is thermodynamically favorable. Furthermore, Mg and Si atoms tend to be adsorbed on the surface firstly where the E_{ads} is larger. From Table 2, it can be observed that, for AlP(1 0 0) surface, Mg and Si atoms prefer to be adsorbed on P-terminated AlP(1 0 0) firstly. However, for AlP(3 3 1), Mg and Si atoms would like to be adsorbed on top-site of Al atoms preferentially. On the initial stage, Mg and Si atoms in Al–Mg_2Si melt surround AlP particles randomly. Because of the interaction between Mg, Si atoms and AlP(1 0 0) or (3 3 1), Mg and Si atoms tend to be adsorbed on the AlP as an adsorbed layer. In the layer, Mg and Si atoms can be arranged. As temperature decreases, the adsorbed layer transforms into Mg_2Si crystal driven by undercooling and AlP/Mg_2Si interfaces are formed in term of adsorption model [30,31]. AlP particles can act as high efficiency nucleating agent for primary Mg_2Si. As a result, primary Mg_2Si particles change from coarse dendrite to fine octahedron/truncated octahedron by increase of the Mg_2Si crystal nuclei.

Conclusion

In this paper, experimental observation and theoretical calculation were carried out to reveal the heterogeneous nucleation potential of AlP for primary Mg_2Si in Al–Mg_2Si alloys. The interfacial atomic structure, work of adhesion (W_{ad}), electronic structure of AlP(1 0 0)/Mg_2Si(2 1 1) and AlP(3 3 1)/Mg_2Si(1 1 0) interfaces were investigated using first-principles calculations. The main conclusions are summarized as follows:

(1) For AlP(1 0 0)/Mg_2Si(2 1 1) and AlP(3 3 1)/Mg_2Si(1 1 0) interfaces, the W_{ad} exhibits the following sequence: P-terminated AlP(1 0 0)/Mg_2Si(2 1 1) interface (4.13 J/m^2) > Al-terminated AlP(1 0 0)/Mg_2Si(2 1 1) interface (2.73 J/m^2) > AlP(3 3 1)/Mg_2Si(1 1 0) interface (1.03 J/m^2).
(2) For P-terminated AlP(1 0 0)/Mg_2Si(2 1 1) interface, the chemical bonds are formed between the interfacial Mg, Si atoms of Mg_2Si side and P atom of AlP side. For AlP(3 3 1)/Mg_2Si(1 1 0) and Al-terminated AlP(1 0 0)/Mg_2Si(2 1 1) interfaces, there is a only relatively weak chemical bond between interfacial Si atom of Mg_2Si side and Al atom of AlP side.
(3) The morphologies of primary Mg_2Si particles change from coarse dendrite to fine octahedron/truncated octahedron (~20 μm), due to the existence of AlP as the effective heterogeneous nucleus of Mg_2Si.

Acknowledgments

This work was supported by a grant from National Natural Science Foundation of China (No. 51404169 and No. 51774212), National Science Fund for Distinguished Young Scholars of China (No. 51325401) and Natural Science Foundation of Tianjin (No. 15JCQNJC03200). The calculation work was carried out at National Supercomputer Center in Tianjin, and the calculations were performed on TianHe-1 (A). The authors are grateful to Associate Professor Enzuo Liu at Tianjin university for his calculation discussion.

Appendix A. Supplementary data

Supplementary data associated with this article can be found, in the online version, at https://doi.org/10.1016/j.rinp.2017.11.025.

References

[1] Wang L, Qin XY. The effect of mechanical milling on the formation of nanocrystalline Mg_2Si through solid-state reaction. Scripta Mater 2003;49:243–8.
[2] Li GH, Gill HS, Varin RA. Magnesium silicide intermetallic alloys. Metall Trans A 1993;24:2383–91.
[3] Li C, Wu YY, Li H, Liu XF. Morphological evolution and growth mechanism of primary Mg_2Si phase in Al–Mg_2Si alloys. Acta Mater 2011;59:1058–67.
[4] Chen L, Wang HY, Luo D, Zhang HY, Liu B, Jiang QC. Synthesis of octahedron and truncated octahedron primary Mg_2Si by controlling the Sb contents. CrystEngComm 2013;15:1787–93.
[5] Azarbarmas M, Emamy M, Rassizadehghani J, Alipour M. M. karamouz, The influence of beryllium addition on the microstructure and mechanical properties of Al–15%Mg_2Si in-situ metal matrix composite. Mater Sci Eng A 2011;528:8205–11.
[6] Bai GZ, Liu Z, Lin JX, Yu ZF, Hu YM, Wen CE. Effects of the addition of lanthanum and ultrasonic stirring on the microstructure and mechanical properties of the in situ Mg_2Si/Al composites. Mater Des 2016;90:424–32.
[7] Emamy M, Khorshidi R, Raouf AH. The influence of pure Na on the microstructure and tensile properties of Al–Mg_2Si metal matrix composite. Mater Sci Eng A 2011;528:4337–42.
[8] Li ZD, Li C, Gao ZM, Liu YC, Liu XF, Guo QY, Yu LM, Li HJ. Corrosion behavior of Al–Mg_2Si alloys with/without addition of Al–P master alloy. Mater Character 2015;110:170–4.
[9] Tebiba M, Samuela AM, Ajerschb F, Chen XG. Effect of P and Sr additions on the microstructure of hypereutectic Al–15Si–14Mg–4Cu alloy. Mater Character 2014;89:112–23.
[10] Nasiri N, Emamy M, Malekan A, Norouzi MH. Microstructure and tensile properties of cast Al–15%Mg2Si composite: effects of phosphorous addition and heat treatment. Mater Sci Eng A 2012;556:446–53.
[11] Zhao YG, Qin QD, Liang YH, Zhou W, Jiang QC. In-situ Mg_2Si/Al–Si–Cu composite modified by strontium. J Mater Sci 2005;40:1831–3.
[12] Li C, Liu XF, Wu YY. Refinement and modification performance of Al–P master alloy on primary Mg_2Si in Al–Mg–Si alloys. J Alloys Compd 2008;465:145–50.
[13] Nordin NA, Farahany S, Ourdjini A, Abu Bakar TA, Hamzah E. Refinement of Mg_2Si reinforcement in a commercial Al–20%Mg_2Si in-situ composite with bismuth, antimony and strontium. Mater Charact 2013;86:97–107.
[14] Vaziri Yeganeh SE, Razaghian A, Emamy M. The influence of Cu–15P master alloy on the microstructure and tensile properties of Al–25wt% Mg_2Si composite before and after hot-extrusion. Mater Sci Eng A 2013;566:1–7.

[15] Rashba EI. Theory of electrical spin injection: tunnel contacts as a solution of the conductivity mismatch problem. Phys Rev B 2000;62:R16267–70.
[16] Toth GI, Tegze G, Pusztai T, Granasy L. Heterogeneous crystal nucleation: the effect of lattice mismatch. Phys Rev Lett 2012;108:025502.
[17] Zhao XB, Zhuo YG, Liu S, Zhou YF, Zhao CC, Wang CX, Yang QX. Investigation on WC/TiC interface relationship in wear-resistant coating by first-principles. Surf Coat Technol 2016;305:200–7.
[18] Dai JH, Song Y, Yang R. Influence of alloying elements on stability and adhesion ability of $TiAl/TiO_2$ interface by first-principles calculations. Intermetallics 2017;85:80–9.
[19] Yang J, Huang JH, Fan DY, Chen SH. First-principles investigation on the electronic property and bonding configuration of NbC (111)/NbN (111) interface. J Alloys Compd 2016;689:874–84.
[20] Liu S, Zhou YF, Xing XL, Wang JB, Yang QX. Refining effect of TiC on primary M_7C_3 in hypereutectic Fe–Cr–C harden-surface welding coating: experimental research and first-principles calculation. J Alloys Compd 2017;691:239–49.
[21] Wang HL, Tang JJ, Zhao YJ, Du J. First-principles study of Mg/Al_2MgC_2 heterogeneous nucleation interfaces. Appl Surf Sci 2015;355:1091–7.
[22] Han YF, Dai YB, Shu D, Wang J, Sun BD. First-principles calculations on the stability of Al/TiB_2 interface. Appl Phys Lett 2006;89:144107.
[23] Kresse G, Joubert D. From ultrasoft pseudopotentials to the projector augmented-wave method. Phys Rev B 1999;59:1758–75.
[24] Hafner J. Ab-initio simulations of materials using VASP: density-functional theory and beyond. J Comput Chem 2008;29:2044–78.
[25] Perdew JP, Burke K, Ernzerhof M. Generalized gradient approximation made simple. Phys Rev Lett 1996;77:3865–8.
[26] Bramfitt BL. The effect of carbide and nitride additions on the heterogeneous nucleation behavior of liquid iron. Metall Trans 1970;1:1987–95.
[27] Monkhorst HJ, Pack JD. Special points for Brillouin-zone integrations. Phys Rev B 1976;13:5188–92.
[28] Momma K, Izumi F. VESTA 3 for three-dimensional visualization of crystal, volumetric and morphology data. J Appl Crystallogr 2011;44:1272–6.
[29] Siegel DJ, Hector Jr LG, Adams JB. Adhesion stability and bonding at metal/metal-carbide interfaces: Al/WC. Surf Sci 2002;498:321–36.
[30] Chalmers B. Principles of solidification. New York: Springer Science + Business Media; 1964.
[31] Kim WT, Cantor B. An adsorption model of the heterogeneous nucleation of solidification. Acta Metall Mater 1994;42:3115–27.